Review of Scientific Instruments ARTICLE scitation.org/journal/rsi

In-fiber Michelson interferometric sensor fabricated by single CO_2 laser pulse

Cite as: Rev. Sci. Instrum. 93, 095004 (2022); doi: 10.1063/5.0092947
Submitted: 24 March 2022 • Accepted: 24 August 2022 •
Published Online: 26 September 2022

Qiang Zhang,[1,2,a] Chunzheng Wang,[1] Yanyu Guo,[1] Yuhao Li,[1] Quansen Wang,[1] Doudou Wang,[1] and Yongmin Li[1,2,a]

AFFILIATIONS

[1] State Key Laboratory of Quantum Optics and Quantum Optics Devices, Institute of Opto-Electronics, Shanxi University, Taiyuan 030006, China
[2] Collaborative Innovation Center of Extreme Optics, Shanxi University, Taiyuan 030006, China

[a] **Authors to whom correspondence should be addressed:** qzhang@sxu.edu.cn and yongmin@sxu.edu.cn

ABSTRACT

An in-fiber Michelson interferometric sensor was presented by fabricating a concavity on the end face of a single mode fiber using a single CO_2 laser pulse. Reflected beams from the bottom and air–cladding boundary of the concavity are coupled into the fiber core and superimpose to generate a two-beam in-fiber Michelson interferometer. Compared with other laser-machining methods where multiple scanning cycles with precise manipulation are needed, the proposed method is more straightforward because only a single laser pulse is used to construct the sensor. The concavity constructed by the CO_2 laser is very smooth, and its shape could be controlled flexibly by changing the position of the single mode fiber and the parameters of the CO_2 laser pulse, so the fringe visibilities of the proposed sensors could be more than 15 dB, which is higher than that of the most reported laser-machining in-fiber Michelson interferometers. The proposed sensor was demonstrated by measuring the temperature with a sensitivity of 11.13 pm/°C. Furthermore, the proposed device is compact (<100 μm), economical, and robust. These advantages make it a promising candidate in practical applications.

I. INTRODUCTION

Optical fiber sensors have played important roles in various exciting applications, such as operando stress monitoring in lithium-based batteries,[1] optofluidic manipulation,[2,3] and aircraft structure health monitoring.[4] As one of the significant fiber-optic interferometers, various fiber-optic Michelson interferometers (MIs) have been demonstrated experimentally.[5–18] Most traditional fiber-optic MIs are constructed by using the two optical fibers as the sensing and reference arms, respectively.[5,6] Compared with the MIs with two fibers, in-fiber MIs are promising in practical applications owning to the advantages of compact size, high stability, and easy operation.[7–18] To construct in-fiber MIs, many artful methods have been proposed. A common approach is to employ special optical fibers, such as Hi-Bi optical fiber,[7] thin-core optical fiber,[8] and two-core optical fiber.[9] Those special fibers require complicated fabrication techniques,[10] and the costs are expensive. Another common method is to fabricate special interference structures using fusion splicing technology, such as core-mismatching joint,[11] abrupt taper,[12] sphered-end hollow fiber,[13] cone-shaped inwall capillary,[14] and peanut structures,[15] which unfortunately have poor repeatability and accuracy due to the manual operation. Recently, laser processing technology with excellent repeatability and accuracy has been applied to fabricate in-fiber MIs, such as cutting off a half of the fiber core[16,17] and fabricating inclined narrow slits[10,18] by a femtosecond laser. However, in order to achieve sufficient visibility of the in-fiber MIs by a femtosecond laser, multiple scanning cycles with precise manipulation of the fiber and femtosecond laser are needed.[10,16–18] Furthermore, the surface by a femtosecond laser is rough, and the cost of the processing equipment is high. Therefore, it is meaningful to develop novel laser processing technologies for in-fiber MIs.

In this work, we presented a new method to construct an in-fiber MI by evaporating the end face of a standard single mode fiber (SMF) to fabricate a concavity using a single CO_2 laser pulse. The reflected light at the concavity includes two beams. One beam is reflected by the bottom of the concavity to the SMF core directly. The other beam is reflected to the SMF cladding at the side of the

concavity and then returns to the core of the SMF through the air–cladding boundary and the side of the concavity. Both reflected beams superimpose to generate a two-beam in-fiber MI. The proposed method has the following advantages. First, only a single CO_2 laser pulse is used to fabricate the in-fiber MI, so the fabricating process is very straightforward compared to the femtosecond-laser processing methods. Second, a high fringe visibility of the MI could be achieved because of the smooth shape-controllable concavity. Experimental test data showed that the fringe visibility of the in-fiber MI could be more than 15 dB, which is higher than that of the most reported laser-machining in-fiber Michelson interferometers. The proposed sensor was demonstrated by measuring the temperature with a sensitivity of 11.13 pm/°C. Moreover, the cost of the proposed processing setup is much less than that using a femtosecond laser. Therefore, the proposed method is promising for practical applications.

II. OPERATION PRINCIPLE

The operating principle of the in-fiber MIs is presented in Fig. 1. A smooth shape-controllable concavity is fabricated on the end face of the fiber by the CO_2 laser. When light emanating from a laser is transmitted to the concavity, the reflected light includes two parts: one part is reflected by the bottom of the concavity, and the other part is reflected by the side of the concavity and the air–cladding boundary. The two reflected beams superimpose to generate a two-beam MI. The light powers of the two beams can be controlled flexibly by optimizing the shape of the concavity. Here, we ignore the effect of the light reflected from the core–cladding boundary due to small difference of refractive indices between the core and the cladding of SMF (fiber: Corning's SMF-28e, n_{eff} is 1.4682, and refractive index difference is 0.36%).

The normalized reflection power of the in-fiber MI could be expressed as

$$I = A^2R + B^2R + 2ABR \times \cos\frac{2\pi n_f \Delta L}{\lambda}, \tag{1}$$

$$A = (1-\alpha_1)\beta_1, \tag{2}$$

$$B = (1-\alpha_2)^2(1-\alpha_3)\beta_2, \tag{3}$$

$$R = \left(\frac{n_f - n_a}{n_f + n_a}\right)^2, \tag{4}$$

FIG. 1. Operating principle of the in-fiber MI.

where n_a and n_f are the refractive indices of air and the optical fiber; α_1, α_2, and α_3 are the losses of three mirrors (such as roughness), respectively; R is the reflection coefficient between the fiber and air; ΔL is the difference between the two arms; β_1 and β_2 are the coupling coefficients of reflected beams, respectively; and λ is the wavelength.

According to the operating principle of the proposed device shown in Fig. 1, the bottom area and the position with an incident angle of 45° for the concavity depend on the depth and width of the concavity, so the relative intensities of the two beams and the fringe visibility of the reflection spectrum are relevant to the depth and width of the concavity. There is an optimal width (depth) for the maximum fringe visibility when the depth (width) is constant. However, the sensitivity of the sensor is irrelevant to the depth and width of the concavity according to Eq. (5). To achieve higher fringe visibility, the theoretical optimal width and depth of the concavity could be obtained by equalizing the two reflected beams from the bottom and side of the concavity. The cross section of the concavity is a Gaussian curve,[19]

$$f(x) = -ae^{-\frac{2(x-b)^2}{c^2}}, \tag{5}$$

where a and c are the depth and width of the concavity and b is the location of the concavity. The position with an incident angle of 45° for the concavity could be achieved according to Eq. (5). Considering the refractive index difference (RID) of the SMF-28e, the acceptable ranges of the incident angles from the bottom and side of the concavity are −2.43°–2.43° and 43.785°–46.215°, respectively. By integrating and equalizing the optical intensities of the corresponding bottom and side areas of the concavity, the theoretical optimal width and depth could be obtained. Figure 2 shows the simulated normalized fringe visibilities as functions

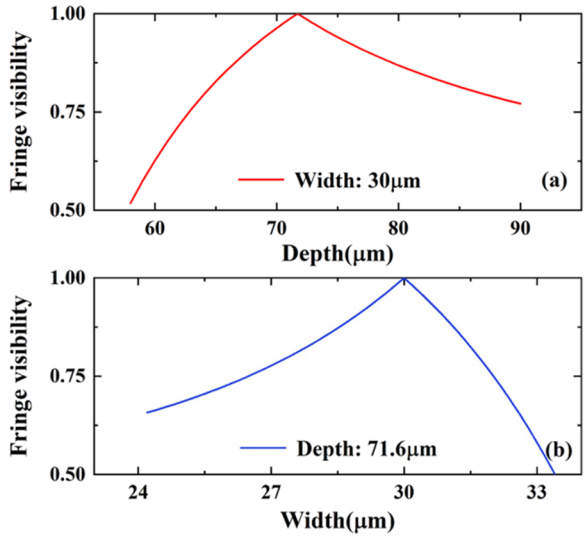

FIG. 2. Simulated normalized fringe visibilities for the concavities with different depths (a) and widths (b).

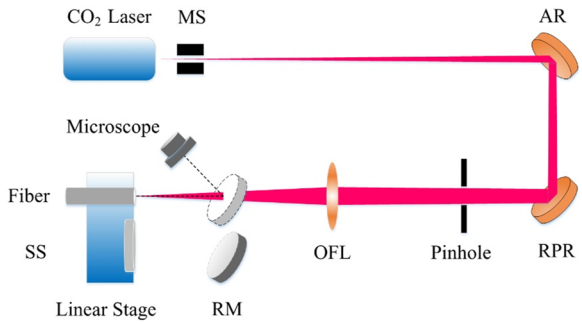

FIG. 3. Fabricating system for the in-fiber concavity.

of the depth (a) and width (b) when the width and depth are 30 and 71.6 μm, respectively. As shown in Fig. 2, the fringe visibility decreases when the value deviates from the corresponding optimal value. In experiments, the concavity with optimal width and depth could be fabricated by optimizing the relative position between the end face of SMF and the beam waist, and the characteristic parameters of the CO_2 laser pulse (including the intensity and pulse length).

The proposed in-fiber MIs could be used to measure environmental temperature fluctuation, and the temperature sensitivity of the proposed in-fiber MI can be expressed as[20]

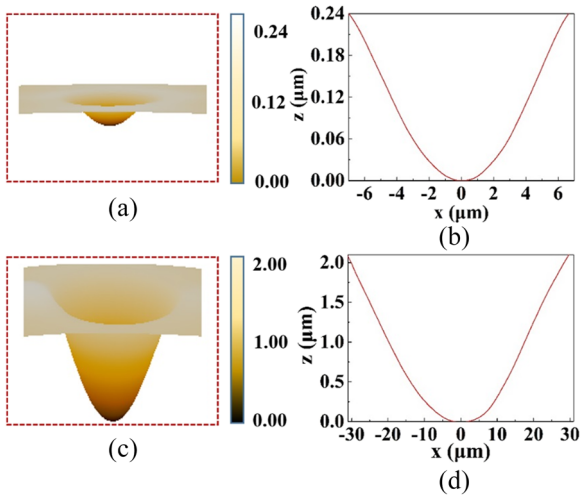

FIG. 5. (a) and (c) AFM images of the concavities. (b) and (d) Corresponding section lines of the concavities.

$$S = \frac{\partial \lambda}{\partial T} = \left(\frac{1}{n_f}\frac{\partial n_f}{\partial T} + \frac{1}{\Delta L}\frac{\partial \Delta L}{\partial T}\right)\lambda = (\alpha_T + \zeta_T)\lambda, \tag{6}$$

where α_T and ζ_T are the thermo-optic coefficient and thermal expansion coefficient of optical fibers. It is obvious that the temperature fluctuation can be obtained in real time by measuring the resonant-wavelength shift.

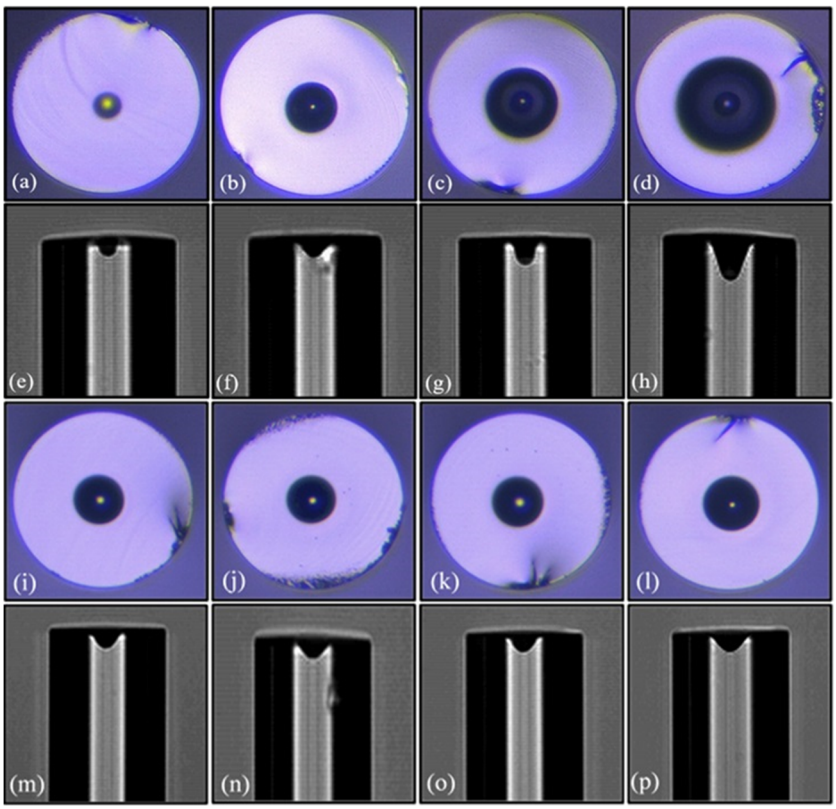

FIG. 4. (a)–(d) End faces of the concavities with diameters of 16, 32, 48, and 64 μm, respectively. (e)–(h) Side views of the corresponding depths of 18, 23, 28, and 47 μm, respectively. (i)–(l) End faces of the concavities with diameters of 33.08, 32.76, 33.16, and 33.96 μm, respectively. (m)–(p) Side views of the corresponding depths of 19.19, 18.65, 19.50, and 19.93 μm, respectively.

III. FABRICATING PROCESS

The fabricating process of the proposed in-fiber MI is quite straightforward. Figure 3 shows the fabricating system of the in-fiber concavity on a SMF, consisting of a CO_2 laser (L4S, Access laser), a mechanical shutter (MS), an absorbing reflector (AR, II–VI Incorporated), an optical focusing lens (OFL, II–VI Incorporated), a reflective phase retarder (RPR, II–VI Incorporated), a silica substrate (SS), a reflecting mirror (RM, II–VI Incorporated), and a precision linear stage (Newport). First, the CO_2 laser is turned on to produce a continuous wave laser with a wavelength of 10.6 μm, which passes through the MS and is converted into a laser pulse with adjustable pulse length. Then, the pulse laser is projected on the AR mirror, where p-polarized light is absorbed and s-polarized light is reflected. The s-polarized pulse laser converted light into circularly polarized light by the RPR mirror. Compared with linearly polarized or non-polarized light, there are two main advantages for circularly polarized light. First, the concavity fabricated by the circularly polarized light could optimize the ellipticity of the concavity because absorption of the material is dependent on the polarization direction of the light.[21] Second, using circularly polarized light can prevent the formation of ripples.[22] The pinhole is used to produce a clean Gaussian beam. The circularly polarized light is focused on a SMF by the OFL to construct an in-fiber concavity, where the SS and optical microscope are applied to adjust the relative position between the SMF and the pulse laser.[23]

The shape of the in-fiber concavity could be controlled flexibly by changing the relative position between the end face of SMF and the beam waist, and the characteristic parameters of the CO_2 laser pulse (including the intensity and pulse length). Figures 4(a)–4(d)

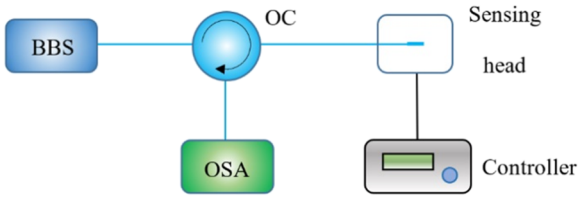

FIG. 6. Michelson interferometer sensing experimental system.

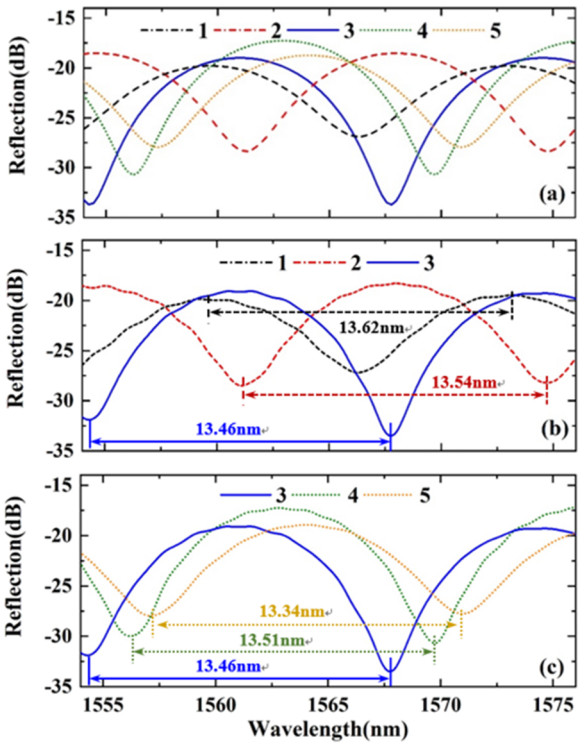

FIG. 7. (a) Simulated reflection spectra of the in-fiber MIs and (b) measured reflection spectra of the in-fiber MIs with the same width of 30 μm and different depths of 56 μm (1), 82 μm (2), and 71 μm (3). (c) Measured reflection spectra of the in-fiber MIs with the same depth of 71 μm and different widths of 30 μm (3), 27 μm (4), and 33 μm (5).

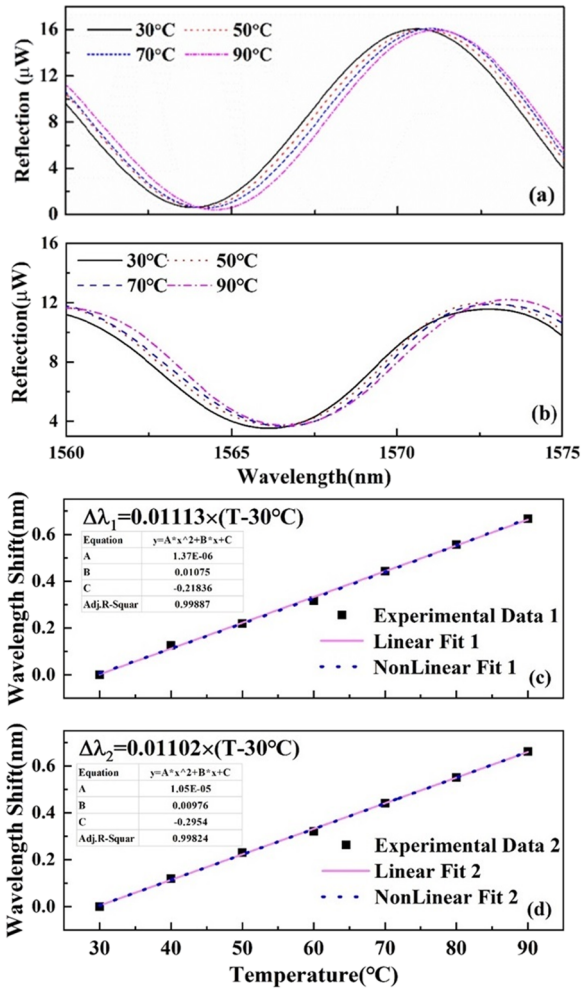

FIG. 8. (a) and (b) Reflection spectra and (c) and (d) dip wavelength evolution of the in-fiber MIs with different temperatures.

show four representative optical images of the concavities with different fabricating parameters of (0 μm, 0.8 W, 20 ms), (50 μm, 1 W, 30 ms), (100 μm, 1.2 W, 40 ms), and (150 μm, 1.4 W, 50 ms) (referring to the relative position between the end face of SMF and the beam waist, and the intensity and pulse length of the CO_2 laser pulse). For our experimental setup, the width of the concavity could be tuned from 10 to 100 μm and the corresponding depth from 0.1 to 80 μm. In addition, the in-fiber MI sensor has good repeatability. Figures 4(i)–4(p) show four representative optical images of the concavities with same fabricating parameters (60 μm, 1 W, 25 ms). One of the advantages of this method is that only a single CO_2 laser pulse is used to fabricate the in-fiber MI. It is very straightforward compared with the femtosecond-laser processing methods, where several scanning cycles with precise manipulation are needed. Moreover, the CO_2 laser in our experiments is of less cost than a femtosecond laser. Therefore, the proposed method is promising for practical applications.

Meanwhile, a low roughness reflector is essential for fiber-optic interferometers to obtain high-visibility interference and large reflected power. Figure 5 shows the AFM images and the corresponding section lines of the concavities. Experimental results show that the roughness of the concavity fabricated by the CO_2 laser is far lower than that using a femtosecond laser.[10,16–18]

IV. EXPERIMENTAL RESULTS AND DISCUSSION

In our experiments, a lot of in-fiber MIs with different widths and depths were fabricated. Figure 6 shows the whole test system for the in-fiber MIs, including a broadband source (BBS), a fiber-optic circulator (OC), an optical spectrum analyzer (OSA203, Thorlabs), and a temperature-controlled oven. Using the above system, several in-fiber MIs with the same depth (width) and different widths (depths) were measured. As shown in Figs. 7(b) and 7(c), the clear two-beam interference fringes could be obtained. Because the concavity is smooth and its shape can be changed by optimizing the position of the SMF and parameters of the CO_2 laser pulse, the measured fringe visibilities are up to 15 dB, which is higher than that of most laser-machined in-fiber MIs.[10,17,18] The corresponding FSRs are 13.62 nm (1), 13.54 nm (2), 13.46 nm (3), 13.51 nm (4), and 13.34 nm (5), which are consistent with that of the parameters of SMF. To illustrate the experimental results, we simulated reflective spectra of the MIs based on Eq. (1) with α_1 = 0.1, 0.1, 0.1, 0.1, 0.1, α_2 = 0.1, 0.1, 0.1, 0.1, 0.1, α_3 = 0.1, 0.1, 0.1, 0.1, 0.1, 0.2, β_1 = 0.53%, 0.74%, 0.85%, 1%, 0.7%, β_2 = 1.7%, 1.8%, 1.5%, 1.9%, 1.8%, ΔL = 124.352 μm, 123.884 μm, 123.331 μm, 123.484 μm, 122.510 μm, and R = 0.036 for the five reflected spectra in Fig. 7(a), respectively. The experimental results are consistent with the simulated spectra.

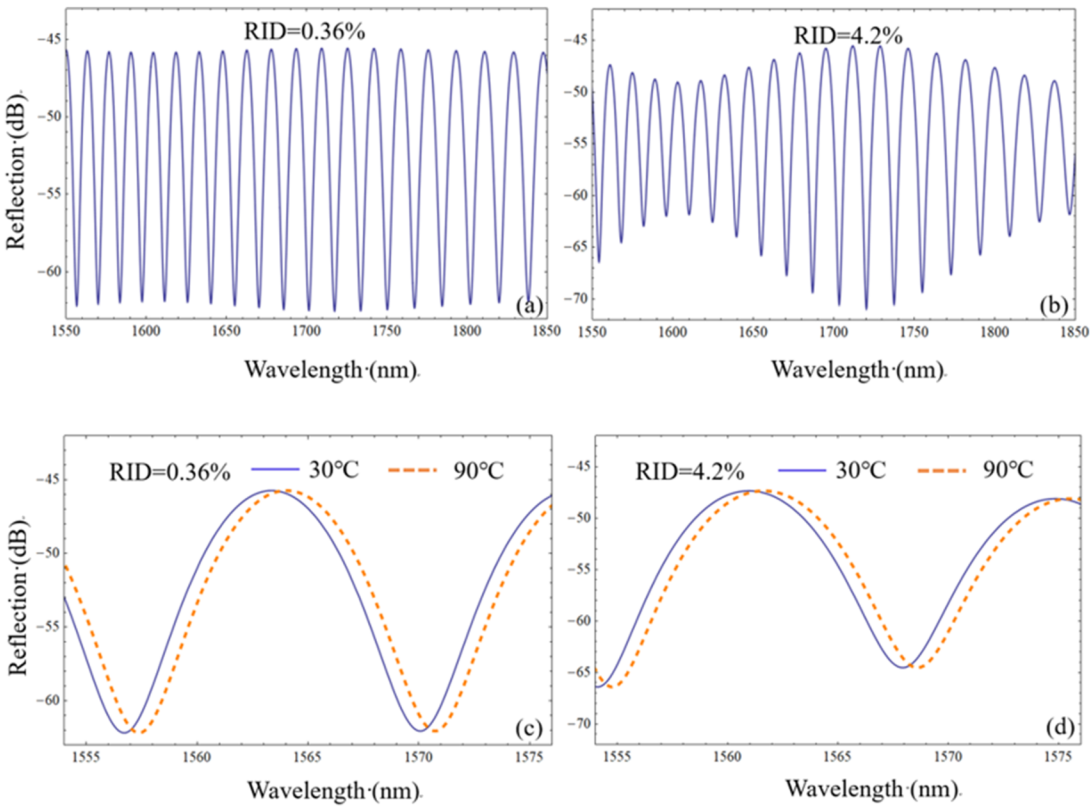

FIG. 9. Reflection spectra of the in-fiber MIs with RID of 0.36% (a) and 4.2% (b) and shifts of reflection spectra for the in-fiber MIs with RID of 0.36% (c) and 4.2% (d) at different temperatures.

To corroborate the proposed in-fiber Michelson interferometers in practical applications, we measured the responses of the MI sensors to the temperature fluctuation by placing the in-fiber MI sensors in the oven. As shown in Figs. 8(a) and 8(b), the reflection spectra of MIs with different parameters ($Diameter_a$ = 15 μm, $Depth_a$ = 33 μm; $Diameter_b$ = 23 μm, $Depth_b$ = 46 μm) will shift regularly (red shift) with the increase of temperature from 30 to 90 °C. The shape of the fiber-optic concavity affects the resonant wavelength and fringe visibility of the MI sensor. According to Eq. (5), the redshift of the resonant wavelength is from the thermal expansion and thermo-optic effect. The evolutions of the dip wavelengths (λ_a = 1570.58 nm and λ_b = 1566.12 nm) were traced to analyze the temperature sensitivities of the in-fiber MIs further. As shown in Figs. 8(c) and 8(d), the data points of the wavelength shifts of MIs with temperature are fitted with linear and second-order polynomial curves, where the non-linear correlation coefficients (R2) of (c) and (d) are 0.998 87 and 0.998 24, and the linear correlation coefficients (R2) are 0.999 89 and 0.999 78, respectively. The sensitivities of the two sensors with linear fitting are 11.13 and 11.02 pm/°C, which are close to the sensitivities of 11.34 and 11.31 pm/°C simulated by Eq. (5) ($\alpha_T = 6.67 \times 10^{-6}$, $\zeta_T = 0.55 \times 10^{-6}$). Similar experimental results were observed for other in-fiber MIs.

The reflected light from the core–cladding boundary will turn the two-beam interference model to a three-beam interference model when the refractive index difference (RID) between the core and cladding for some special fibers is much larger than that of a standard SMF (Corning's SMF-28e, RID is 0.36%). According to the three-beam interference theory,[24] the fringe visibility of the reflected spectrum will be changed obviously as the reflected light from the core–cladding boundary increases. As shown in Figs. 9(a) and 9(b), the simulated fringe visibility changes when the RID increases from 0.36% to 4.2%. Meanwhile, Figs. 9(c) and 9(d) show that the shifts of the reflected spectra are insensitive to the changes of the RID.

V. CONCLUSION

In this work, we proposed an in-fiber MI sensor based on a concavity on a SMF, which is fabricated by a single CO_2 laser pulse. The reflected light at the concavity includes two beams: one beam is from the bottom of the concavity and couples into the fiber core, and the other beam is reflected by the side of the concavity into the fiber cladding and then returns to the core of the SMF through the air–cladding boundary and the concavity. The two beams form the in-fiber MI. Experimental test data showed that the fringe visibility of the in-fiber MI could be more than 15 dB because of the smooth shape-controllable concavity. Compared with the methods based on a femtosecond-laser, the proposed method using a CO_2 laser is more straightforward, because only a single CO_2 laser pulse is used. Moreover, the cost of the proposed processing setup is much less than that using a femtosecond laser. Therefore, the proposed method is a promising candidate for practical applications.

ACKNOWLEDGMENTS

This work was supported by the funding from the National Natural Science Foundation of China (NSFC) (Grant Nos. 12174232, 11804208, U21A6006, and 11774209) and Shanxi 1331KS.

AUTHOR DECLARATIONS

Conflict of Interest

The authors have no conflicts to disclose.

Author Contributions

Qiang Zhang: Conceptualization (lead); Funding acquisition (equal); Investigation (equal); Methodology (equal); Project administration (equal); Supervision (equal); Writing – original draft (equal); Writing – review & editing (equal). **Chunzheng Wang**: Data curation (equal); Investigation (equal); Methodology (equal); Software (equal); Writing – original draft (equal). **Yanyu Guo**: Formal analysis (equal); Investigation (equal); Software (equal); Validation (equal); Visualization (equal); Writing – original draft (equal). **Yuhao Li**: Data curation (equal); Formal analysis (equal); Investigation (equal); Methodology (equal); Software (equal); Validation (equal). **Quansen Wang**: Data curation (equal); Formal analysis (equal); Investigation (equal); Software (equal); Validation (equal); Visualization (equal). **Doudou Wang**: Formal analysis (equal); Methodology (equal); Resources (equal); Software (equal); Validation (equal). **Yongmin Li**: Conceptualization (equal); Funding acquisition (equal); Project administration (equal); Resources (equal); Supervision (equal).

DATA AVAILABILITY

The data that support the findings of this study are available from the corresponding author upon reasonable request.

REFERENCES

[1] L. A. Blanquer, F. Marchini, J. R. Seitz, N. Daher, F. Bétermier, J. Huang, C. Gervillié, and J.-M. Tarascon, Nat. Commun. **13**, 1153 (2022).
[2] X. Yang, C. Gong, C. Zhang, Y. Wang, G. F. Yan, L. Wei, Y. C. Chen, Y. J. Rao, and Y. Gong, Laser Photonics Rev. **16**, 2100171 (2022).
[3] L. Li, Y. Zhang, Y. Zhou, W. Zheng, Y. Sun, G. Ma, and Y. Zhao, Laser Photonics Rev. **15**, 2000526 (2021).
[4] I. García, J. Zubia, G. Durana, G. Aldabaldetreku, M. Illarramendi, and J. Villatoro, Sensors **15**, 15494 (2015).
[5] S. DeWolf, F. K. Wyatt, M. A. Zumberge, and W. Hatfield, Rev. Sci. Instrum. **86**, 114502 (2015).
[6] M. Rhodes, J. Catenacci, M. Howard, B. La Lone, N. Kostinski, D. Perry, C. Bennett, and J. Patterson, Rev. Sci. Instrum. **89**, 035111 (2018).
[7] J. Zhang, H. Sun, R. Wang, D. Su, T. Guo, Z. Feng, M. Hu, and X. Qiao, IEEE Sens. J. **13**, 2061 (2013).
[8] J. Zhou, Y. Wang, C. Liao, B. Sun, J. He, G. Yin, S. Liu, Z. Li, G. Wang, X. Zhong, and J. Zhao, Sens. Actuators, B **208**, 315 (2015).
[9] F. Peng, J. Yang, X. Li, Y. Yuan, B. Wu, A. Zhou, and L. Yuan, Opt. Lett. **36**, 2056 (2011).
[10] J. Liu and D. N. Wang, Opt. Lett. **43**, 4304 (2018).
[11] H. Cao and X. Shu, IEEE Sens. J. **17**, 3341 (2017).
[12] Z. Tian, S. S.-H. Yam, and H.-P. Loock, Opt. Lett. **33**, 1105 (2008).
[13] N.-K. Chen, K.-Y. Lu, J.-T. Shy, and C. Lin, Opt. Lett. **36**, 2074 (2011).
[14] X. Zhang, H. Bai, H. Pan, J. Wang, M. Yan, H. Xiao, and T. Wang, IEEE Photonics J. **10**, 6801808 (2018).
[15] D. Wu, T. Zhu, and M. Liu, Opt. Commun. **285**, 5085 (2012).
[16] L. Yuan, T. Wei, Q. Han, H. Wang, J. Huang, L. Jiang, and H. Xiao, Opt. Lett. **37**, 4489 (2012).

[17]C. R. Liao, D. N. Wang, M. Wang, and M. Yang, IEEE Photonics Technol. Lett. **24**, 2060 (2012).
[18]Y. Liu and D. N. Wang, IEEE Photonics Technol. Lett. **30**, 293 (2018).
[19]D. Hunger, C. Deutsch, R. J. Barbour, R. J. Warburton, and J. Reichel, AIP Adv. **2**, 012119 (2012).
[20]P. Chen and X. Shu, Opt. Express **26**, 5292 (2018).
[21]M. Uphoff, M. Brekenfeld, G. Rempe, and S. Ritter, New J. Phys. **17**, 013053 (2015).
[22]F. Keilmann and Y. H. Bai, Appl. Phys. A **29**, 9 (1982).
[23]Q. Zhang, Z. Fan, J. Zhang, F. Zhang, Q. Zhang, and Y. Li, Appl. Opt. **59**, 8959 (2020).
[24]J. Tian, Y. Jiao, S. Ji, X. Dong, and Y. Yao, Opt. Commun. **412**, 121 (2018).